IEEE Access
Multidisciplinary | Rapid Review | Open Access Journal

Received August 9, 2020, accepted August 15, 2020, date of publication September 9, 2020, date of current version September 22, 2020.

Digital Object Identifier 10.1109/ACCESS.2020.3022943

An Unsupervised Retinal Vessel Segmentation Using Hessian and Intensity Based Approach

MUSAED ALHUSSEIN[1], KHURSHEED AURANGZEB[2], (Senior Member, IEEE), AND SYED IRTAZA HAIDER[2]

[1]Department of Computer Engineering, College of Computer and Information Sciences, King Saud University, Riyadh 11543, Saudi Arabia
[2]College of Computer and Information Sciences, King Saud University, Riyadh 11543, Saudi Arabia

Corresponding author: Khursheed Aurangzeb (kaurangzeb@ksu.edu.sa)

The authors extend their appreciation to the Deputyship for Research & Innovation, Ministry of Education in Saudi Arabia for funding this research work through the project number (*DRI-KSU-*415).

ABSTRACT The structure of blood vessels play a crucial role in diagnoses of the various vision threatening diseases including Glaucoma and Diabetic Retinopathy (DR). The correct segmentation of retinal blood vessels is a crucial step in the study of retinal fundus images. We proposed a simple unsupervised approach by using a combination of Hessian based approach and intensity transformation approach. We have applied CLAHE for enhancing the contrast of the retinal fundus images. An enhanced version of PSO algorithm is applied for contextual region tuning of CLAHE. Morphological filter and Wiener filter are used to de-noise the enhanced image. The eigenvalues are obtained from the Hessian matrix at two different scales to extract thick and thin vessel enhanced images separately. The intensity transformation approach is separately applied to the enhanced image to maximize the vessel details. Global Otsu thresholding is applied on intensity transformed image and thick vessel enhanced image whereas ISODATA local thresholding is applied on thin vessel enhanced image. Finally, a simple post-processing step based on the region parameters such as area, eccentricity, and solidity is used. The region parameters are obtained for each connected component in input binary images. The threshold values of region parameters are empirically investigated and applied to each of the three binary images to remove the non-vessel components. The thresholded images are combined by applying logical OR operator, which resulted in the final segmented binary image. We assessed our developed framework on the open-access CHASE_DB1 and DRIVE datasets, achieving a sensitivity of 0.7776 and 0.7851, and an accuracy of 0.9505 and 0.9559 respectively. These results outperform several state-of-the-art unsupervised methods. The reduced computational complexity and significantly improved evaluation metrics advocates for its use in the automated diagnostic systems for retinal image analysis.

INDEX TERMS Machine learning, vessel segmentation, CLAHE, morphology, Wiener filter.

I. INTRODUCTION

The long term diabetes leads to Diabetic retinopathy (DR). The DR is one of the main sources of blindness in working age populations. The preliminary symptoms of this disease are lesions which, is a general term connecting different terminologies including hard/soft exudates, microaneurysms (MA), dot/blot hemorrhages, inter retinal microvascular abnormalities and leakages. The ophthalmologists grade the disease by evaluating the number, types and severity of the various kinds of lesions on retina. This growths of the DR towards blindness is gradual and the main issue is that the individual does not feel the signs in the initial phases. The DR is considered as one of the main cause of vision loss specifically in the young peoples with diabetes [1].

For an ophthalmologist, one of the initial symptom of DR is MA that mainly happen due to leakage from blood vessels on the retinal surface. The MAs are circular in shape and red in color and appear as small circular dots on the retinal surface. When the walls of MAs are broken then the hemorrhages are formed on the retinal surface. When the blood which leak from retinal blood vessels contains proteins and lipids then the exudates are formed, which can lead to full blindness if it is accumulated near the macula. The

The associate editor coordinating the review of this manuscript and approving it for publication was Hao Ji.

This work is licensed under a Creative Commons Attribution 4.0 License. For more information, see https://creativecommons.org/licenses/by/4.0/

exudates are bright lesions while the MAs and the haemorrhages are usually the dark lesions [2]. The internal structure of human-eye is composed of various parts such as iris, vessels, macula, vitreous, optic cup, optic disc, pupil, cornea etc. Among the various parts of eye, the vessels are significantly important for analysing and grading various diseases such as DR [3], [4].

The fundoscopy is usually applied for capturing images of the internal structure of the eye (retina). The images captured by using the fundoscopy plays an important role in diagnosing various eye diseases. The complex optical system of fundoscopy is composed of many lenses which provides a telescopic view of the retinal structure [5]. Usually, the ophthalmologists manually grade the retinal fundus images which, is a time consuming and cumbersome task. Additionally, the manual analysis of the retinal fundus images by the ophthalmologist may contain substantial variations because of the interference and exhaustion. Contrarily, machine learning based automated approaches for retinal analysis have the potential for higher accuracy in addition to capability for large scale public screening. Mainly, there two types of machine learning methods which are supervised and unsupervised. The unsupervised approaches utilize the hidden features in the images for retinal image segmentation and their most favourable advantage is that such methods do not require the manually marked huge database for training. These approaches classify the pixels of an image into vessels or non-vessels without any priori knowledge. Contrarily, the supervised approaches learns based on the features in the input images and the associated manually marked gold standard images.

The accuracy of the automated approaches for retinal vessels segmentation is substantially improved based on the unparallel advancement in artificial intelligence (AI) and supervised as well as unsupervised machine learning (ML). Furthermore, the machine learning based approaches for retinal vessels segmentation has the potential to be employed in the automated system for large scale deployment. The large scale deployment of the machine learning based automated system is substantially crucial for timely detection of eye sicknesses [6].

The researchers have recently developed many automated system for large scale deployment in public screening programs. The efficient implementation of these automated system is crucial for the early detection of numerous diseases. The implementation of these automated system involves various tasks such as the detection of optic disc/cup [7], [8] and retinal vessels [9], [10]. The performance and reliability of the automated public screening system is substantially important because of the health of the general public. For aiming to develop an efficient and effective automated system for eye diseases, the developed machine learning models should be investigated appropriately and their robustness in mimicking the skills of the expert ophthalmologists must be ensured. This imply proper investigation of efficient methods for vessels and optic disc/cup segmentation [7]–[10].

The performance of developed automated system for eye disease classification is directly depended on the performance of the selected machine learning method for detecting the vessels, the lesions and the optic cup/disc. Among these detection tasks, the vessels segmentation has been widely accepted as a challenging problem and is the highly important part of the eye sickness diagnosis system [11]. The various attributes of the retinal vessels including the density, the tortuosity, the size and the length are significantly important and affects the performance of the developed method. Additionally, the centerline reflex, the branching, the crossing and the changing direction of the vessels adds to the complexity of the vessel segmentation problem. Moreover, the numerous parts of the retina including the macula, optic cup, the optic disc, the vitreous, the iris and the different kinds of lesions such as the soft exudates, hard exudates also significantly increase the complexity of the automated eye disease classification system. These set of factors stances many defies for the automated eye disease classification system.

The focus of this work is retinal vessels segmentation and we have selected the unsupervised category due to their many advantages including reduced computational complexity, no hyper parameters tuning, lower memory requirements and most importantly the specialized hardware is not needed for the training the developed algorithm. The unsupervised methods classify the pixels in a retinal image without any ground truth images, which is a huge plus point, as such a large database is usually not available for large scale screening program. The techniques in the unsupervised category learns based on the vessels attributes hidden in the retinal images.

The following are the main contributions of our work.

- The contrast of the retinal fundus images is enhanced by applying the PSO based technique for tuning the contextual region of CLAHE.
- The Top-Hat transformation and the Wiener filter are applied for de-noising the enhanced image image.
- Intensity transformation is applied for maximizing the vessel details.
- Thick and thin vessels are extracted from the enhanced images by utilizing eigenvalues from Hessian matrix. Two different sigma's are selected for obtaining images with thin and thick vessels.
- Global Otsu thresholding and ISODATA thresholding are applied for binarizing the enhanced images obtained through different methods.
- The threshold values of region parameters (area, eccentricity and solidity) are empirically investigated and applied to remove the non-vessel components.

The remaining manuscript is divided into various sections as follows. The section 2 provides the literature review and the section 3 explains the proposed unsupervised vessel detection approach. The experimental results along with a comparison (comprehensive) with existing representative methods in the field are provided in section 4. Some of the important

results are discussed in section 5. Lastly, the conclusion is presented in section 6.

II. RELATED WORK

The existing state of the art on retinal vessel segmentation is categorised into supervised and unsupervised machine learning approaches [12]. In this section, the most recent and relevant vessels segmentation approaches separated in these two categories are briefly discussed. For a recent detailed review of retinal vessel segmentation techniques please refer to [13].

Unsupervised methods utilize the hidden features in the images for retinal image segmentation. The most favourable benefit of unsupervised machine learning techniques is their functionality without the requirement for the manually marked huge database for training. The unsupervised methods classify the pixels of an image into vessels or non-vessels without any priori knowledge. Recently, numerous researchers have explored different unsupervised machine learning approaches for retinal vessels segmentation. The unsupervised machine learning approaches commonly have three stages: pre-processing; the main techniques (segmentation algorithm); the post-processing. A detailed review of these vessels segmentation methods is provided by the authors in [14], where they divided these techniques into six categories: (1) kernel based approaches; (2) tracking (vessel) approaches; (3) morphological; (4) multiscale; (5)adaptive local thresholding (6) model based. They also divided these techniques into two major classes generally known as rule based (also called unsupervised techniques) and machine learning. The methods in the rule based class obey some rules and regulations for separating the retinal vessels in retinal images. Contrarily, the methods in the machine learning class, are trained using a large database of ground truth retinal fundus images.

The idea of a kernel-based approach (also called the matched filtering approach) is to apply a 2D filter kernels for mapping the vessels in the retinal image. Usually, the Gaussian-shaped filters are applied for modeling the retinal vessels. In [15], the authors proposed a method using a set of twelve directional kernels along with a threshold probing technique to segment the retinal vessels. The main issue with the kernel-based filtering approaches is their tendency to highlight the non-blood vessel section of the images, which significantly degrade the overall performance of the system.

Different variants of matched filtering approach are proposed in [16]–[18], and [19]. In [16], a hybrid matched filtering technique was proposed. In the matched filter phase, symmetric Gaussian kernel was used to detect the vessels whereas, in the thresholding phase, the first-order derivate of Gaussian was used to establish a dynamic threshold. Most of the matched filtering approach variants focus on improving the thresholding technique rather than improving the matched filter kernel. One of the major limitations of the matched filtering approach is based on an assumption that along with a certain distance, the width of retinal vessels is constant. This assumption limits the adaptability of the matched filtering approach to the variation in retinal vessel width and orientation. In [20], the authors combine the responses of many shifted filters and obtained substantially better evaluation metrics. However, their segmentation method may present limitations on images with pathologies.

The tracking-based approaches trace the ridges of the retinal images with the help of a set of starting points [21]. The ridge detection requires a pre-processing step to enhance vessels of different width and orientations. The main issue with tracking-based approaches is the high dependency of ridge detection on the pre-processing steps. Another limitation of tracking-based approaches is that it requires user intervention for choosing the starting and endpoints, thus they are not fully automatic.

The morphology approaches apply the mathematical equations for retinal vessel segmentation. Generally, the Top-hat operators are applied for detecting the retinal vessels. In [22], authors used curvelet transform and morphological operators to enhance the edges and ridges of the retinal images respectively. The method was only tested on a single database. In [23], the authors used a combination of morphological and topological operators to segment the retinal vessels.

The diameter of the blood vessels is bigger at the origin (Optic Disc) and slowly decreases outward. For extracting the size, the width, and the orientations of the retinal vessels in retinal images, multi-scale methods are better options as these methods can analyze the shape and intensity of the blood vessels at various scales [24], [25]. In [25], the authors used Gabor wavelet and multi-scale line detector for retinal vessel segmentation. The method performed well in segmenting the thick vessels. However, for fine vessel segmentation, it results in over-segmentation. In general, the multi-scale methods are faster but their accuracy is degraded by the non-vessel parts in the images.

The authors in [26] explored an adaptive thresholding based technique for segmenting retinal vessels. A drawback of adaptive thresholding based technique is that it sometimes results in unconnected vascular structure.

Model-based approaches segment the vessel in the retinal images by considering them as flexible curves using curve evolution [27]. This method performs poorly due to unsegmented thin vessels resulting in low sensitivity (0.6634). In [28], the authors proposed a segmentation method based on multiconcavity modeling. The method is too sensitive to intra-image contrast variation. In addition, the authors didn't evaluate various performance metrics such as sensitivity and specificity. The authors in [29] also applied a hybrid region (model-based) approach for separating retinal vessels from retinal images. Their approach performed better for fine vessel detection that is a highly challenging task. However, the computational complexity of the method is very high.

The above mentioned unsupervised retinal vessel segmentation methods revealed their novel performances. However, the existing techniques may face challenges in accurately detecting the retinal vessels from the fundus images when

there is uneven illumination, intensity inhomogeneity, image blurring, and low contrast. Recently proposed unsupervised techniques have achieved significant progress in vessel segmentation. However, there are a few aspects that need to be addressed to further improve segmentation accuracy. For example, vessel connectivity, thick and thin vessel class imbalance, intra-image contrast variability, and fine vessel segmentation. The proposed segmentation method should ensure high vessel connectivity with less computation as well as high segmentation accuracy in detecting the thick and thin vessels.

Semi-supervised methods

Some researchers have even applied hybrid approaches by combing two methods for achieving better evaluation metrics. One example is [30], in which the authors proposed a hybrid approach based on a combination of GMM and morphological method. Their hybrid method is comprised of three steps. Initially, they used the green channel for extracting the binary image. Then high pass filters in combination with morphology are applied on the binary image. In the second stage, the major vessels were extracted. Then the GMM classifier and a set of eight features are used for pixel classification. In the final stage of the hybrid approach, the extracted major vessels are combined with the classified vessel pixels (GMM based pixel classification). The hybrid technique achieved better evaluation metrics on both normal and pathological retinal images and it is also computationally efficient.

The authors [31] also adopted a hybrid machine learning approach, in which they used AdaBoost classifier in combination with matched filtering for retinal vessel segmentation. For contrast enhancement of the images, they used the CLAHE. Then the morphological filter were applied on the contrast enhanced images. They applied the Frangi filters and B-COSFIRE for improving the detected vessels. They fed a number of statistical features to the AdaBoost classifier in order to extract the vessel. Finally, some post-processing operations were also performed for neglecting the incorrectly detected pixels.

Supervised machine learning models learns based on the attributes and features in the input images and the associated manually graded golden images manually graded by experienced optometrists/ophtalmologists. The developed models are trained and tested using the manually graded retinal fundus image datasets. The developed and trained models are applied for the classification of the retinal vessel. Recently, various researchers have implemented supervised machine learning models for segmenting vessels for diagnosing different diseases. Some notable examples are diagnoses of the glaucoma, the retinal vascular occlusions and the DR [4], [32]–[35]. Although the supervised machine learning approaches have achieved significantly better evaluation metrics for various tasks such as vessels detection and optic cup/disc detection [7]–[10] but unsupervised machine learning approaches are still being explored and preferred because of their lower computational complexity and no requirement of manually marked retinal image databases, in addition to many constraints of the supervised machine learning approaches.

Though some machine learning models have achieved marginally better accuracy compared to that of the unsupervised approaches but they do have many constraints which limit their applicability. The main limitations of the supervised machine learning models is that their classification accuracy is proclaimed by the availability of a manually graded publicly available database, its size and features. Most importantly, the substantially higher computational complexity linked with the training and testing of the multi-layered deep model in addition to hyper parameter tuning and large memory overhead hinder its feasibility for deployment in public screening program. Contrarily, the unsupervised machine learning approaches do not require database of ground truth images and most importantly their computational complexity is significantly low. Furthermore, no model training and hyper parameter tuning is involved. Due to these attributes of the unsupervised machine learning models, researchers show keen interest in their explorations for various applications.

III. PROPOSED METHOD

In current section of the manuscript, we will elaborate our developed unsupervised vessel segmentation approach. Figure 1 presents the flowchart of developed framework. We split RGB retinal image into green, red, and blue parts and extract the green image. In our proposed method, we perform the following noteworthy steps;

- Improved PSO technique is used for the contextual region tuning of CLAHE for retinal vessel contrast enhancement.
- Top-Hat transformation is applied on inverted CLAHE image for the removal of noisy objects.
- Wiener filter is applied for de-noising the image.
- Intensity transformed image is obtained by applying gamma correction to maximize the vessel details.
- Thick and thin vessels enhanced images are obtained by utilizing eigenvalues from Hessian matrix. Two different sigma's are selected for obtaining images with thin and thick vessels.
- Global Otsu method is selected for thresholding the intensity transformed image and thick vessel enhanced image whereas ISODATA thresholding is applied on thin vessel enhanced image.
- Region parameters such as area, eccentricity and solidity are obtained for each connected component in input binary images. The threshold values of region parameters are empirically investigated and applied to remove the non-vessel components. This step is repeated for all the three binary images, i.e. intensity transformed binary image, thick vessel binary image and thin vessel binary image. The logical OR operation is performed on the thresholded images for obtaining the final segmented image.

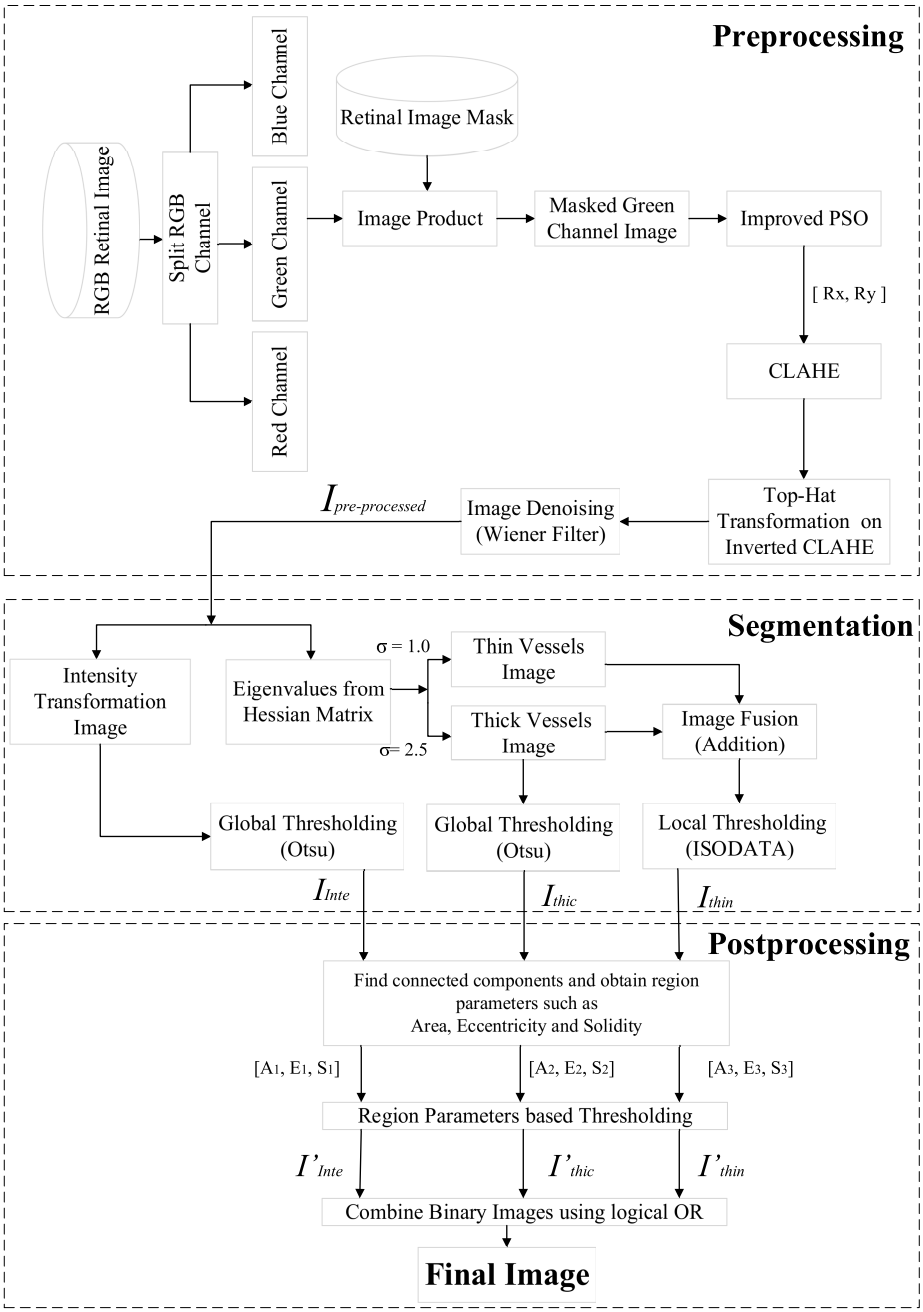

FIGURE 1. Flowchart of the proposed vessel segmentation algorithm.

A. PRE-PROCESSING

Three pre-processing steps including contrast enhancement using PSO based CLAHE, morphological Top-Hat transformation and Wiener filtering are performed, which are explained with details below.

1) PSO–CLAHE FOR CONTEXTUAL REGION TUNING

Contrast enhancement is a fundamental pre-preprocessing step to improve the details in the captured image. The CLAHE is a well-known local contrast enhancement technique that requires rectangular contextual region defined as (Rx, Ry) and a clip limit (Cl) as parameters. In [36] and [3], authors have used CLAHE for vessel contrast enhancement with default parameters i.e. contextual region as (8, 8) and clip limit as 0.01. However, the retinal images often exhibit contrast variability within and across images. Thus, it is not appropriate to use the default parameters of CLAHE for each retinal image. Instead of using a fixed window size, we have used our modified PSO algorithm from [37] as an optimizer to adaptively select the contextual region of CLAHE for retinal image contrast enhancement

Algorithm : Modified PSO for Determining Optimal Contextual Regions for CLAHE

Initialize the following parameters:

Number of Particles ($\boldsymbol{P = 25}$), Dimension ($\boldsymbol{D = 2}$), Iterations ($\boldsymbol{Ite = 15}$), Function Evaluations ($\boldsymbol{FE = P \times Ite}$), Cognitive Acceleration Constant ($\boldsymbol{c_1 = 2}$), Social Acceleration Constant ($\boldsymbol{c_2 = 2}$), Maximum Inertial Weight ($\boldsymbol{w_1 = 0.5}$), Minimum Inertial Weight ($\boldsymbol{w_2 = 0}$), Maximum Search Space ($\boldsymbol{R_{max} = 32}$), Minimum Search Space ($\boldsymbol{R_{min} = 2}$), Clip Limit ($\boldsymbol{Cl = 0.0198}$)

for $Iter = 1$ **do**

Initialize each particle position $\boldsymbol{X_J}^1$ and particle velocity $\boldsymbol{V_J}^1$ randomly for each dimension within the search space ($\boldsymbol{R_{min}}$, $\boldsymbol{R_{max}}$)

Generate the enhanced image $\boldsymbol{Ie_J}^1$ using CLAHE as transformation function for each particle

Evaluate the fitness value using the fitness function for each $\boldsymbol{Ie_J}^1$ according to equation (1)

Set personal best $\boldsymbol{P_{best\,J}}^1$ and global best $\boldsymbol{G_{best}}^1$

Set $current_{FE} = P$ and $Iter = 1$

end for

while $Iter < Ite$ **do**

for each particle **do**

Calculate the new velocity ${V_J}^{iter}$ according to equation (2)

Calculate the new position ${X_J}^{iter}$ according to equation (4)

for each dimension **do**

if ${X_J}^{iter} > R_{max}$ ***or*** ${X_J}^{iter} < R_{min}$ ***then***

Randomize ${X_J}^{iter}$ within the search space

end if

end for

Generate the enhanced image ${I_{eJ}}^{iter}$ using CLAHE as transformation function for ${X_J}^{iter}$

Evaluate the fitness value using the fitness function for each ${I_{eJ}}^{iter}$ according to equation (1)

Update ${P_{best\,J}}^{iter}$

$current_{FE} = current_{FE} + 1$

Update the inertial weight according to equation (3)

end for

Update G_{best} after each iteration

$Iter = Iter + 1$

end while

FIGURE 2. Algorithm: PSO applied to Contextual Region Tuning of CLAHE for Retinal Image Enhancement.

The PSO is a optimization (population based) heuristic algorithm where the particles move around and change their spatial position with the passage of time. The particles are composed of a velocity vector and a position vector and fly in a multi-dimensional search-space. These particles adjust its position based on its personal experience as well as neighboring particles experience. These particles have their individual fitness parameter that is assessed based on the objective function. In each iteration, particles local best as well as swarms global best is updated. The local and the global best help particles to move to a better solution.

Figure 2 shows the algorithm applied to contextual region optimization of CLAHE for retinal image enhancement. In this work, we are optimizing the contextual region of CLAHE so our search space is 2D, i.e. each particle $X_J = (Rx, Ry)$. In the first iteration, for each particle J, the position vector X_J and the velocity vector V_J is randomly initialized within the search space ($Rmin$, $Rmax$). We then generate an enhanced image I_{eJ} for each particle using CLAHE as a transformation function. Initially, we have adaptively selected the clip limit along with the contextual region using modified PSO. We found that the clip limit for all the fundus images lies in the range of (0.0196, 0.0198). Therefore, a clip limit of 0.0198 is fixed for reducing the execution time of the algorithm. The quality of enhanced image for each particle is evaluated by a fitness parameter which is calculated by applying equation (1) [38].

$$F(I_e) = log(log(E(I_s))).\frac{n_{edges}(I_s)}{M * N}.H(I_e) \tag{1}$$

In equation 1, I_e represents improved image obtained through CLAHE as transformation function, I_s is the edge

image after applying Sobel edge detection method, n_{edges} is the edges count the image (edge), $E(I_s)$ represents accumulated value of the pixel intensities in the edge image, and $H(Ie)$ represent enhanced image's entropy. The objective of applying the modified PSO technique is to obtain the optimum window/tile size of CLAHE by maximizing the fitness function (1). The personal best and the global best for every particle and for the whole the swarm are saved in P_{best} and G_{best} respectively. The velocity vector is then updated based on the value of the local best (every particle) along with the global best (whole swarm) by applying equation (2).

$$\begin{aligned} V_J^{(iter+1)} &= wV_J^{iter} \\ &+c_1r_1(P_{best_j}^{iter} - X_J^{iter}) \\ &+c_2r_2(G_{best}^{iter} - X_J^{iter}) \end{aligned} \tag{2}$$

In equation (2), c_1 is the the cognitive constant while c_2 is the social acceleration constants, w is the inertial weight which is calculated using equation (3), and r_1 and r_2 are random numbers (uniformly distributed).

$$w = w_{max} - \frac{w_{max} - w_{min}}{FE} * current_{FE} \tag{3}$$

where w_{max}, w_{min}, FE and $current_{FE}$ denotes the maximum inertial weight, the minimum inertial weight, the function evaluations and the current function evaluations respectively. The inertial weight is iteratively decreased to gradually reduce the impact of particle's previous velocity and to increase the impact of local and global search. The new position of each particle is then calculated using equation (4).

$$X_J^{(iter+1)} = X_J^{iter} + V_J^{(iter+1)} \tag{4}$$

In [37], we proposed particle penalization to ensure that the particles do not fly outside the search space. In this work, we check if for each particle, the new position vector is within the search space. If any of the dimension is out of the search space then we randomize that particular dimension to update the position vector. For the remaining iterations, for each particle, the updated position vector is passed to the transformation function to obtain the enhanced image and then evaluate the fitness value based on the objective function. The local best and the global best parameter are updated after each iteration. The stopping criteria for the optimization problem is the function evaluations expressed as equation (5)

$$FE = P * Ite \tag{5}$$

where P and Ite are number of particles and number of iterations respectively. Figure 3 presents a comparison (visual) between CLAHE with default contextual region and CLAHE with PSO based optimized contextual region which can be observed in Figure 3 (b) and (c) respectively. The Figure 3 (a) is the green channel image of test Image1 from DRIVE database. In Figure 2 (c), it can be seen that the retinal vessels (specifically the ones near the optic disk and the thin vessels) are more enhanced from the background as compare to Figure 3 (b).

FIGURE 3. Test Image1 from DRIVE database. (a) Green Channel Image. (b) CLAHE with default contextual region. (c) CLAHE with PSO based contextual region optimization.

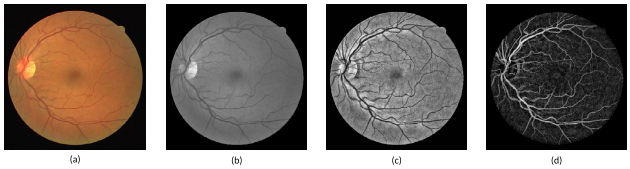

FIGURE 4. Image from DRIVE database. (a) Original RGB Image. (b) Green Channel Image. (c) Enhanced Image using PSO-CLAHE. (d) Morphological Top-Hat on Inverted CLAHE image.

2) MORPHOLOGICAL TOP-HAT TRANSFORMATION

Our next pre-processing step is applying the Top-Hat transformation to inverse image generated in the previous step. The mathematical equation for the Top-Hat transformation is given in equation (6).

$$I_{TH} = I_C - (I_C \circ S) \tag{6}$$

where I_{TH} is the Top-Hat transformed image, I_C is the complementary image,and S is the structuring element. In this paper, we have considered a disk type structuring element with a radius of eleven pixels. The morphological top-hat transformation extracts the object that is smaller than the structuring element. The width of other structures such as exudates and the optic disk is usually more than the width of the widest retinal vessel. Therefore, the top-hat will enhance only the retinal vessels and suppresses the intensity variation due to possible exudates and optic disk. Compared to the red and blue image components, the blood vessels are more clearer in the green channel.Therefore, in this work, we selected the green image. Figure 4 (d) shows the Top-Hat transformed image where the retinal blood vessels are more prominent than the optic disk and the background and possible exudates are removed.

3) WIENER FILTER

We have applied wiener filter as our final step (preprocessing). It is noise-removal (adaptive) low-pass filtering technique that is based on statistical estimation of neighborhood pixels of size M-by-N. The wiener filter calculates the local mean and variance of a neighborhood. If the variation is high, the filter applies weaker smoothing whereas if the variation is low, the filter applies stronger smoothing. In this work, we have used the default parameters of wiener filter. As shown in Figure 5 (b), wiener filter suppresses the noise in the enhanced image.

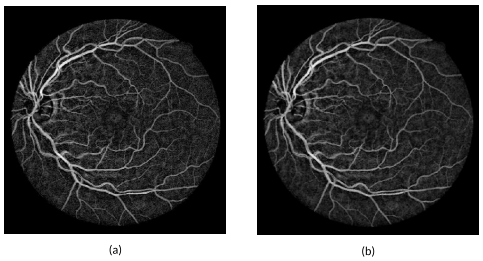

FIGURE 5. Morphological operator and Wiener Filter responces (a) Top-Hat Transformation on inverted CLAHE image. (b) Wiener filter enhanced image.

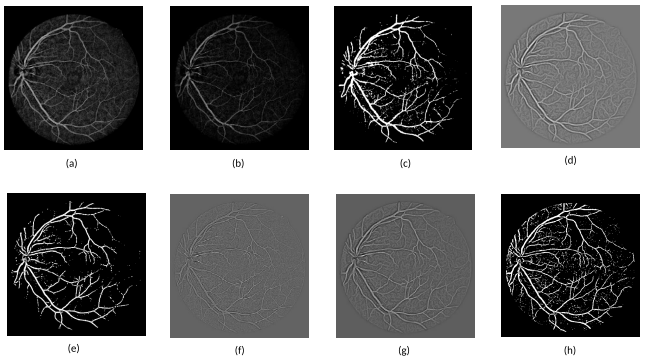

FIGURE 6. Images at various stages of the algorithm. (a) Wiener filter enhanced image. (b) Intensity transformed image. (c) Intensity transformed binary image. (d) Thick vessel enhanced image. (e) Thick vessel binary image. (f) Thin vessel enhanced image. (g) Fused Image of thin and thick vessel enhanced image. (h) Thin vessel binary image.

B. SEGMENTATION

In the last pre-processing stage, we have applied Wiener filtering for obtaining enhanced image which is passed as input to the segmentation step for further processing as shown in Figure 6 (a).

We have segmented the retinal vessels in two distinct methods as shown in Figure 1. The first method is to obtain the intensity transformed image by applying power-law transformation on the input image to the segmentation step, to highlight the retinal vessels. The second method is to apply eigenvalues transformation and hessian matrix approach at two different scales to compute the second derivative for the enhancement of thick and thin vessels. We have applied global Otsu algorithm (for thresholding) on the intensity transformed image and thick vessel image (enhanced) to obtain the binary images. For thin vessel enhanced image local ISODATA thresholding is applied.

1) INTENSITY TRANSFORMED IMAGE

In the pre-processing stage, we have applied PSO-CLAHE for enhancing the contrast of images by tuning the contextual region of CLAHE. In the segmentation stage, we first obtain the intensity transformed image by applying power-law transformation to further enhance the retinal vessels and suppress the background. The power-law transformation is also known as gamma correction, mathematically expressed equation (7).

$$T = I^{\eta} \tag{7}$$

In equation (7), the I denotes input image that must be scaled from the range [0, 255] to [0, 1], T is the transformed image and η is a parameter that represents gamma factor that must be positive. The $\eta > 1$ and $\eta < 1$ represents the mapping towards darker and brighter output values respectively.

For enhancing the vessels and suppressing the background, we set a constant gamma factor to 1.5 for all the retinal images. Figure 6 (b) shows the intensity transformed image. We can see that the vessels are enhanced in transformed image whereas the background is suppressed. We have applied Otsu global thresholding on the transformed image to get binary image in Figure 6(c).

2) EIGENVALUES TRANSFORMATION AND HESSIAN MATRIX APPROACH

In the second method, we have obtained improved images of thick and thin retinal vessels by applying Hessian function and finding its eigenvalues. For a grayscale image with intensity values represented in 2-D, the Hessian is a second-order partial derivative square matrix computed as equation (8).

$$H(x, y) = \begin{bmatrix} h_{xx} & h_{xy} \\ h_{yx} & h_{yy} \end{bmatrix} = \begin{pmatrix} \frac{\partial^2 I}{\partial x \partial x} & \frac{\partial^2 I}{\partial x \partial y} \\ \frac{\partial^2 I}{\partial y \partial x} & \frac{\partial^2 I}{\partial y \partial y} \end{pmatrix} \tag{8}$$

The Hessian is a symmetric matrix where h_{xy} is the same as h_{yx}. The Hessian matrix contains the structure information of the grayscale image.Next, we have used eigenvalues transformation to get the structure information of the image. We have obtained eigenvalues λ_1 and λ_2 from the Hessian matrix sorted by absolute values such that $|\lambda_1| > |\lambda_2|$. We have applied differencing approach [36] to obtain two different enhanced images. To obtain the thick and thin vessel enhanced images, the values of σ are set to 2.5 and 1 respectively. Figure 6 (d) and (f) shows the thick and thin vessel enhanced images respectively. We have applied Otsu global thresholding on the thick vessel enhanced image to obtain the binary image as shown in Figure 6 (e). Next, we have fused the thick vessel enhanced image with the thin vessel enhanced image to obtain a single image with having the thin and thick vessels become more prominent as shown in Figure 6 (g). We have applied ISODATA local thresholding technique on a single enhanced image to obtain the thin vessel binary image as shown in Figure 6 (h). ISODATA is an iterative method for threshold selection to discriminate between foreground and background [39]. A block size of [64, 48] non-overlapping has been used for the local thresholding. In order to suppress the noise in the image, we have added an offset (small value) in the threshold. In the segmentation stage, we have obtained three binary images as shown in Figure 6 (c), (e) and (h). We have passed these binary images to the post-processing stage to remove the non-vessel components and obtain the final segmented image.

C. POST-PROCESSING

The inputs to the post-processing block are intensity transformed binary image I_{Inte}, thick vessels binary image I_{thic}, and thin vessels binary image I_{thin} as shown in Figure 7 (a), (b) and (c) respectively. The final step of retinal blood vessel segmentation is the removal of non-vessel components from each of the input binary image. To achieve this, we first obtain the connected components in each of the binary image and then take into consideration the geometric structural properties of those connected regions to filter out the non-vessel components. These region parameters are features whereby thresholds can be empirically investigated or learned using artificial intelligent techniques. In this work, we consider area, eccentricity and solidity as region parameters to empirically obtain the thresholds to remove the non-vessel components from the input binary images. The area is defined as the total pixels count in a region (connected). The solidity is the ratio of connected components area and its convex hull. The eccentricity is the ratio of distance from the center to the foci and the distance from the center to the vertex. As the retinal vessels are elongated patches, therefore, for each connected component to be a vessel, the area should be high, the eccentricity should be close to one, and the solidity should be low. We investigated empirically the region parameters of components (the connected ones) in each of the binary image (input) and made the following observations;

- The components having eccentricity below 0.95 and solidity above 0.40 are anticipated as non-vessels.
- The components that are too large in area (the largest connected component in a binary image) have eccentricity and solidity values well below 0.95 and 0.20 respectively, and are anticipated as vessels.
- The components having area less than 100 pixels are anticipated as non-vessels.

To summarize the post-processing stage, we perform the following steps for each input binary image;

- Find the connected components by adopting Matlab command bwconncomp.
- Obtain the region parameters such as area, eccentricity and solidity using Matlab command regionprop.
- Apply the empirically investigated threshold values of region properties to remove the non-vessel components.

The above mentioned observations helped in determining the threshold values of region parameters. These threshold values were applied separately to each of the input binary image. The final segmented image is then obtained by combining the thresholded images using logical OR operation as shown in Figure 7 (g). We have observed that if the input binary images were fused before applying the empirically calculated threshold values, then it is anticipated with high probability that some vessel components might merge with non-vessel components. This is the reason, we perform the post-processing steps for each input binary image separately.

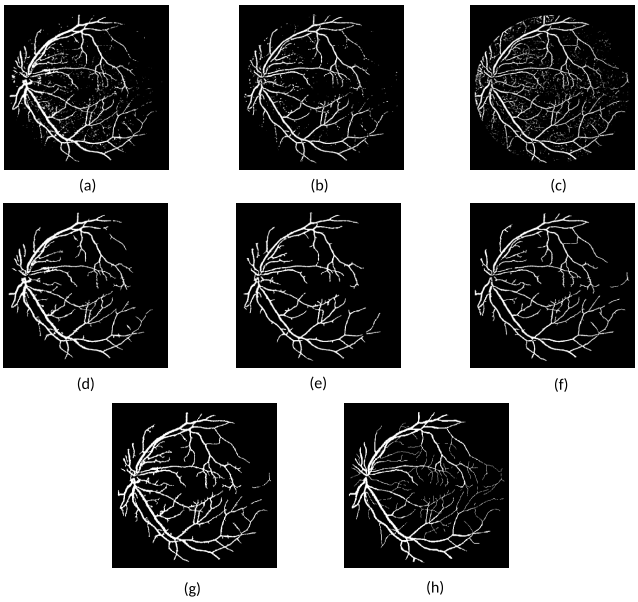

FIGURE 7. Post-processing stages (a) Input intensity transformed binary image IInte. (b) Input thick vessels binary image Ithic. (c) Input thin vessels binary image Ithin. (d) Thresholded intensity transformed binary image I'Inte. (e) Thresholded thick vessels binary image I'thic. (f) Thresholded thin vessels binary image I'thin. (g) Final segmented image by fusing the thresholded images using logical or operation. (h) The ground truth image.

IV. EXPERIMENTAL RESULTS

We have used retinal image databases (DRIVE and CHASE_DB1) for evaluating the performance of the developed unsupervised machine learning approach.

A. DATABASES

The details of the two used retinal image databases are provided below.

1) CHASE_DB1: This is a database of retinal images which covers fourteen pediatric subjects [40]
2) DRIVE: This database contains retinal fundus images covering a wider age range of diabetic patients from Netherlands [41]

In each image of the DRIVE database, the vessel trees are manually segmented. Furthermore, each image is accompanied by a mask in the DRIVE database. The binary mask demarcate the field of view (FOV) and is available only in DRIVE database but is not available for CHASE_DB1 database. Consequently, some well-known methods are applied for creating the masks for the CHASE_DB1 databases [42]. Both the CHASE_DB1 and the DRIVE databases have separate training and testing. We resize the CHASE_DB1 retinal images into the same dimensions as DRIVE retinal images to keep the parameters of the proposed model constant, for example, the radius of the structuring element and eigenvalues transformation.

The details of the two evaluated retinal image databases are provided in the Table 1.

TABLE 1. The details of the two evaluated databases.

Dataset	Dimension in pixels	Dataset Size	Training set	Test set
DRIVE	565 × 584	40	20	20
CHASE_DB1	999 × 960	28	20	8

B. EVALUATION CRITERION

The vessel segmentation approaches are designed and implemented for differentiating between vessels and background. The manually marked ''ground truth'' images are utilized for assessing the developed approach. The four standard evaluation metrics provided below are generally assessed for comparing the performance of the developed method.

1) True Positive (TP): The vessels pixels which are correctly detected by the developed approach
2) False Negative (FN): The vessels pixels which are detected as background pixels by developed approach
3) True Negative (TN): The non-vessels pixels which are detected (correctly) as non-vessels pixels by the developed approach
4) False Positive (FP): The non-vessels pixels detected (incorrectly) as vessels pixels by the developed approach

The parameters provided above are used for evaluating the three main evaluation metrics of the developed approach (For the pixels inside FOV) [17]:

$$Acc = \frac{TP + TN}{TP + FN + TN + FP} \tag{9}$$

$$Se = \frac{TP}{TP + FN} \tag{10}$$

$$Sp = \frac{TN}{TN + FP} \tag{11}$$

$$MCC = \frac{(TP \times TN - FP \times FN)}{\sqrt{(TP+FP)(TP+FN)(TN+FP)(TN+FN)}} \tag{12}$$

The equation (9), (10), (11), and (12) denote accuracy, sensitivity and specificity and MCC respectively. The accuracy is the ratio of the correctly detected pixels (vessels or background) to rest of all pixels in the FOV of the mask. The sensitivity and the specificity measures the detection ratio of the vessel vs non-vessel. The MCC is a balanced accuracy metric that is used to measures the quality of binary classification. It is well suited for problems with class imbalance as it is with the case of retinal vessel segmentation. The MCC values closer to +1 indicates better segmentation method.

C. EVALUATION OF PROPOSED METHOD

The various individual evaluation metrics and their average determined by applying the developed approach on twenty test images of the DRIVE dataset are shown in Table 2. It can be noted that the variation in the sensitivity for the various images is high while it is low for specificity and accuracy.

By performing simulations on the DRIVE database, our overall obtained sensitivity, specificity, accuracy, AUC and MCC are 0.7851, 0.9724, 0.9559, 0.8787 and 0.7481 respectively. The AUC is determined using the equation from [36]. In order to obtain the average values, we run the model for five times. The segmentation results of proposed method on DRIVE database are presented in Figure 8, where the image 1 of the test set is shown in the top row while image 20 is shown in bottom row. In both the rows, the first, second and third columns denote the original image, the ground truth and the segmented image respectively. The various parameters including the TP, FP and FN are indicated using white, red and green colors. The FPs are the results of over-segmentation of the small vessels and some lesions. In column 4 of this figure, it can be observed that, the developed method is capable of detecting most of the blood vessels correctly.

TABLE 2. Evaluation of the Proposed Method on DRIVE database.

Images	Sensitivity	Specificity	Accuracy	AUC	MCC	Time (Sec)
1	0.8621	0.9627	0.9537	0.9124	0.7731	42.44
2	0.8436	0.9663	0.9538	0.9050	0.7753	42.56
3	0.7588	0.9713	0.9501	0.8651	0.7347	42.25
4	0.7609	0.9809	0.9606	0.8709	0.7739	39.87
5	0.7289	0.9810	0.9574	0.8549	0.7540	38.75
6	0.7455	0.9741	0.9518	0.8598	0.7472	41.75
7	0.7454	0.9704	0.9498	0.8579	0.7160	41.19
8	0.7096	0.9791	0.9560	0.8444	0.7200	38.67
9	0.7679	0.9765	0.9596	0.8722	0.7438	41.46
10	0.7737	0.9732	0.9568	0.8734	0.7487	39.95
11	0.7568	0.9666	0.9478	0.8617	0.7158	39.84
12	0.7735	0.9773	0.9597	0.8754	0.7475	40.05
13	0.7516	0.9762	0.9543	0.8639	0.7509	41.46
14	0.8211	0.9670	0.9552	0.8941	0.7304	40.20
15	0.7805	0.9740	0.9601	0.8772	0.7152	37.62
16	0.8181	0.9660	0.9527	0.8920	0.7533	40.85
17	0.7298	0.9843	0.9629	0.8571	0.7480	43.05
18	0.8507	0.9668	0.9576	0.9088	0.7573	40.49
19	0.8806	0.9655	0.9584	0.9230	0.7982	40.22
20	0.8433	0.9680	0.9588	0.9056	0.7578	40.48
Average	**0.7851**	**0.9724**	**0.9559**	**0.8787**	**0.7481**	**40.65**

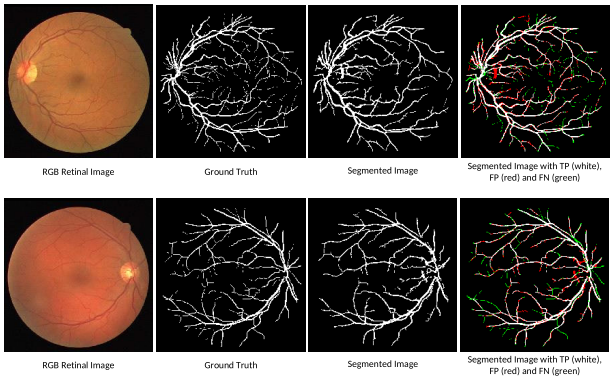

FIGURE 8. Segmentation results of the proposed method on DRIVE dataset. Image 1 (top row) and Image 20 (bottom row).

For the CHASE_DB1 database, we obtained average scores of 0.7776, 0.9634, 0.9505, 0.8705 and 0.6806 for sensitivity, specificity, accuracy, AUC and MCC respectively. The segmentation results of proposed method on CHASE_DB1 database are presented in Figure 9, where the image 13L of the test set is shown in the top row while image 14L is shown in bottom row. We can observe that, the developed method is capable of detecting most of the blood vessels correctly in the representative images of CHASE_DB1 database. As seen in column 4 of Figure 9, there are few FPs that sometimes occur around the optic disk region or certain type of pathologies that present strong contrast.

TABLE 3. The sensitivity, specificity and accuracy of individual as well as various combinations of segmented images in the proposed framework.

Method	DataSet	Sensitivity	Specificity	Accuracy	DataSet	Sensitivity	Specificity	Accuracy
Intensity Transformed	DRIVE	0.6663	0.9866	0.9586	CHASE_DB	0.4657	0.9845	0.9486
Thick Vessel Enhanced		0.6015	0.9891	0.9553		0.5658	0.9839	0.9559
Thin Vessel Enhanced		0.6675	0.9845	0.9565		0.6772	0.9770	0.9567
Intensity Transformed and Thick Vessel Enhanced		0.7179	0.9809	0.9579		0.6447	0.9759	0.9535
Intensity Transformed and Thin Vessel Enhanced		0.7617	0.9770	0.9580		0.7462	0.9705	0.9551
Thick and Thin Vessel Enhanced		0.7263	0.9788	0.9566		0.7292	0.9717	0.9555
Proposed Method - without Wiener filter		0.8100	0.9636	0.9500		0.7884	0.9598	0.9481
Proposed Method - without region parameter thresholding		0.7914	0.9697	0.9540		0.7675	0.9626	0.9490
Proposed Method		0.7851	0.9724	0.9559		0.7776	0.9634	0.9505

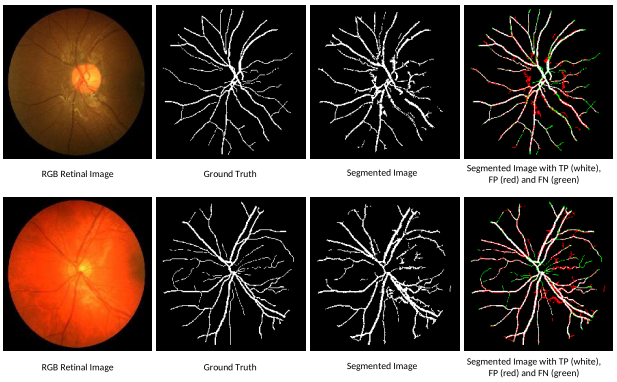

FIGURE 9. Segmentation results of the proposed method on CHASE test dataset. Image 13L (top row) and Image 14L (bottom row).

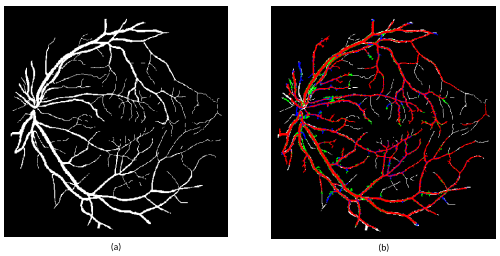

FIGURE 10. Image 12 from DRIVE test database, (a) Ground truth. (b) Segmented Image; Intensity transformed binary image (green), thick vessel enhanced binary image (blue) and thin vessel enhanced binary image (red).

The segmentation results of proposed method on DRIVE dataset for Image 12 are presented in Figure 10, where (a) is the ground truth while (b) is the segmented image. In this figure, the results of the intensity transformation are represented in green while the thick and thin enhanced vessels are shown blue and red respectively. In this figure, each binary image is overlapped to show that the importance of individual contributions from intensity transformed approach as well as Hessian based approach.

V. DISCUSSION

The segmentation and analysis of retinal vascular structure can assist in diagnosing numerous diseases including Glaucoma, DR and hypertension. Usually, the researcher develop automatic methods for studying the variations in various physical parameters including the diameter of blood vessel (retinal), the creation of new retinal blood vessels and the branching of the retinal blood vessels. The accurate segmentation of the vascular structure is crucial due to the fact that the diagnosis of various diseases is dependent on it. But due to the presence of numerous pathologies in retinal images, vascular segmentation is a challenging task.

The segmentation of wide and thin vessels simultaneously is a challenging task because of class imbalance and contrast variability. In [43], the authors examined the ground truth images and observed that around 77% of the vessel pixels belong to thick vessels. This observation was based on an assumption that the vessel pixels belong to a thin vessel if the thickness is less than three pixels. Most of the segmentation methods, especially unsupervised, treat all the vessel

TABLE 4. Comparison with state-of-the-art methods on the DRIVE database.

Type	Methods	Year	Se	Sp	Acc	AUC	MCC
Supervised methods	Second human observer	-	0.7761	0.9725	0.9473	0.8743	-
	[49]	2011	0.7067	0.9801	0.9452	-	-
	[50]	2012	0.7406	0.9807	0.9480	0.8607	-
	[51]	2014	0.7252	0.9798	0.9474	-	-
	[52]	2016	0.7569	0.9816	0.9527	0.8693	-
	[53] FC	2016	0.7893	0.9792	-	0.8791	-
	[53] UP	2016	0.7076	0.9870	-	-	-
	[54]	2017	0.7691	0.9801	0.9533	-	-
	[55]	2018	0.7653	0.9818	0.9542	0.8736	-
	[56]	2019	0.9382	0.9255	0.9271	-	-
	[57]	2019	0.7839	0.9890	0.9709	-	-
	[58]	2020	0.6994	0.9811	0.9450	-	-
Unsupervised methods	[16]	2010	**0.7760**	0.8724	0.9472	0.8422	-
	[28]	2010	-	-	0.9472	-	-
	[22]	2011	0.7352	0.9795	0.9458	-	-
	[59]	2011	0.7410	0.9751	0.9434	-	-
	[60]	2012	0.7030	0.9710	0.9371	0.8370	0.7070
	[40]	2012	0.7152	0.9759	0.9430	0.8607	0.7359
	[20]	2015	0.7655	0.9704	0.9442	0.8680	**0.7475**
	[30]	2015	0.7395	0.9782	0.9494	0.8589	-
	[61]	2015	0.7246	0.9790	0.9403	-	-
	[23]	2016	0.7323	0.9783	**0.9565**	-	0.7245
	[45]	2016	**0.7800**	0.9720	0.9520	**0.8760**	-
	[17]	2016	0.7743	0.9725	0.9476	**0.8754**	-
	[48]	2017	0.7470	**0.9800**	**0.9600**	-	-
	[47]	2017	0.7205	**0.9814**	0.9479	0.8510	-
	[62]	2018	0.7206	0.9757	0.9425	-	0.7400
	[46]	2018	0.7417	**0.9861**	**0.9571**	-	0.6735
	[44]	2019	**0.7800**	0.9401	0.9301	0.8601	-
	[25]	2019	0.7421	0.9773	0.9470	0.8597	**0.7525**
	Proposed Method	2020	**0.7851**	0.9724	0.9559	**0.8787**	**0.7481**

TABLE 5. Comparison with state-of-the-art methods on the CHASE_DB1 database.

Type	Methods	Year	Se	Sp	Acc	AUC	MCC
Supervised methods	Second human observer	-	0.8105	0.9711	0.9545	-	-
	[50]	2012	0.7224	0.9711	0.9569	0.8468	-
	[63]	2014	0.7201	0.9824	0.9530	0.8595	-
	[52]	2016	0.7507	0.9793	0.9581	0.8650	-
	[53] FC	2017	0.7277	0.9712	-	0.8495	-
	[55]	2018	0.7633	0.9809	0.9610	0.8721	-
	[57]	2019	0.7839	0.9894	0.9721	-	-
	[56]	2019	0.9463	0.9364	0.9373	-	-
Unsupervised methods	[40]	2012	0.7224	**0.9711**	0.9469	0.8468	-
	[30]	2015	**0.7615**	0.9575	0.9467	**0.8595**	-
	[20]	2015	0.7585	0.9587	0.9387	0.8586	**0.6802**
	[17]	2016	**0.7626**	**0.9661**	0.9452	**0.8644**	-
	[46]	2018	0.7555	**0.9807**	**0.9521**	-	**0.6614**
	[44]	2019	0.7600	0.9601	**0.9501**	0.8501	-
	Proposed Method	2020	**0.7776**	0.9634	0.9505	**0.8705**	**0.6806**

TABLE 6. Average time for processing one image.

Type	Methods	Year	Processing time	Hardware specification	Software
Supervised methods	[41]	2004	15 min	Pentium 3, 1 GHz, 1 GB RAM	N. A
	[42]	2006	2 min (8 hours Training Time	Pentium 4, 2.1 GHz, 1 GB RAM	Matlab
	[49]	2011	1.5 min	Core 2 Duo CPU 2.13 GHz, 2 GB RAM	Matlab
	[50]	2012	2 min (Training time of 100 s for 200 decision trees)	Core 2 Duo CPU 2.27 GHz, 4 GB RAM	Matlab
Unsupervised methods	[15]	2000	30 s	Pentium-III, 1.5 GHz, 512 MB RAM	Windows Executable
	[41]	2004	15 min	Pentium 3, 1 GHz, 1 GB RAM	N. A
	[64]	2006	2.5 to 3 min	Pentium 4, 3.2 GHz, 960 MB RAM	Matlab
	[28]	2010	13 min	Core 2 Duo 1.83 GHz, 2 GB RAM	Matlab
	[65]	2015	22 s	Core i3 CPU, 2.53 GHz, 4 GB RAM	Matlab, C
	[20]	2015	10 s (DRIVE) 25 s (CHASE_DB1)	2 GHz	Matlab
	[18]	2016	6.4 s	Core i3 CPU, 3.5 GHz, 4 GB RAM	Matlab
	[66]	2017	35 s	Core i5 CPU, 2.6 GHz, 8 GB RAM	C++
	[3]	2019	75 s	Core i7 CPU, 2.21 GHz, 16 GB RAM	Matlab
	[25]	2019	20 s	Core i5 CPU, 6 GB RAM	Matlab
	Proposed	2020	32.48 s (CHASE_DB1) 40.65 s (DRIVE)	Intel Xeon CPU 2.4 GHz, 16 GB RAM	Matlab

pixels with equal importance. It results in a more accurate segmentation of thick vessels as compared to thin vessels. Regarding the contrast variability, the retinal vessels have varying contrast due to which wide vessels (higher contrast) can be extracted easily while it is challenging to extract the thin vessels (poor contrast).

A. OPTIMAL CONFIGURATION OF PROPOSED MODEL

We compare the performance of the developed approach with various combinations of segmented images based on different configurations. Additionally, the performance of the developed approach without Wiener filter as well as without region parameter thresholding is presented. Table 3 shows the performance evaluation of individual as well as various combinations of segmented images using intensity based approach and hessian based approach for thick and thin vessel enhanced images. Table 3 clearly indicates that the proposed method outperforms individual approach based segmented images as well as various combinations of segmented images, especially a combination of thick and thin vessel enhanced image. For the DRIVE and CHASE_DB1 datasets, the sensitivity of the proposed method without Wiener filter is high but the specificity and accuracy are comparatively low.

The performance of the proposed approach is better on the DRIVE dataset than the CHASE_DB dataset as shown in Table 3. In the DRIVE dataset, the classification of the background pixel is better which results in higher accuracy and sensitivity. For the case of CHASE_DB1 dataset, the obtained results are comparable to vast majority of the existing unsupervised machine learning based segmentation approaches. However, slightly lower segmentation accuracy observed in the CHASE_DB1 can be due to problem of central vessel reflection, uneven background illumination or low inter-vessels contrast. The accurate segmentation of CHASE_DB1 database is challenging because of the mentioned attributes of the fundus images.

In another experiment, we evaluated the performance of proposed method without region-based parameter thresholding. We only remove less than or equal to 50 unconnected pixels by considering them as non-vessels then, for DRIVE dataset, we obtain 0.7914, 0.9697, 0.9540, 0.8806, and 0.7275 as sensitivity, specificity, accuracy, AUC and MCC. Table 3 shows that the proposed method (with region parameter thresholding) achieved slightly lower sensitivity but higher specificity, accuracy and MCC. We believe that by incorporating the non-vascular component removal using region parameters thresholding is an optimal post-processing step. It will eliminate the non-vascular components from the segmented image and improve the overall performance of the method.

B. COMPARISON WITH STATE-OF-THE-ART

To assess the performance of our developed framework, we have performed experimentation on two well-known databases that are publicly available i.e. DRIVE and CHASE_DB1. Based on these two databases, we made a comparison between our achieved results and the representative models from the literature. We have taken the values of evaluation metrics of various state-of-the-art methods mentioned in Table 4 and Table 5 from their respective papers. The best three results in each column of the table are highlighted in the red, the green, and the blue which denotes best, second best, and third best results respectively.

From Table 4, it is pertinent that, on the DRIVE database, the sensitivity, accuracy, and AUC of the developed framework is better compared to the second human observer. It can also be observed in the same table that the sensitivity and AUC of the developed framework are the best among the unsupervised approaches respectively. The sensitivity of [44] and [45] are the second-best while that of the [16] third-best among the unsupervised approaches. It is pertinent to note here that [44] and [16] achieved such high sensitivity at the cost of specificity and accuracy. Our obtained specificity is slightly lower than the specificity of [46], [47], and [48] which are the best, the second best and third best among unsupervised methods respectively. The average accuracy of the proposed method lies in fourth place close behind [23] who achieved third-best accuracy at the cost of sensitivity. Talking about MCC, our method outperforms [46] and [23] who achieved best specificity and third-best accuracy respectively. The MCC of our method is in second-place close behind [25].

For the CHASE_DB1 database, from Table 5, it can be observed that the sensitivity, AUC and MCC of the proposed method are the best in the unsupervised approaches. The sensitivity of [17] is the second best while that of the [30] third best among the unsupervised methods respectively. Our obtained specificity is slightly lower than the specificity of [40], [46], and [17] which are the best, the second best and third best among unsupervised methods respectively. It is pertinent to note here that [40] achieved such high sensitivity at the cost of specificity and accuracy. The same local adaptive thresholding technique proposed by Dash [46] scores the highest accuracy with our method in second place. Finally, it should be noted that the AUC and MCC of the proposed method achieved best score among the unsupervised approaches.

From Table 6, the average time required to process one image on a computer with 2.4 GHz CPU and 16 GB RAM for the DRIVE and CHASE_DB1 databases is 40.65 seconds and 32.48 seconds respectively. The different execution time for the two databases is due to the different sizes of the contextual region adaptively selected based on the modified PSO algorithm. The proposed method is computationally efficient and fast comparable to many state-of-the-art methods.

VI. CONCLUSION

We have developed a less computational unsupervised framework for vessel segmentation. Our contributions are mainly in three aspects. First, rather than using default parameters of CLAHE for the contrast enhancement of retinal images, a pre-processing scheme was devised by tuning the contextual region of CLAHE using improved PSO. Second, the Hessian matrix approach and intensity transformation method were separately applied to the pre-processed image to extract the thick and thin vessel enhanced image and intensity transformed image respectively. Third, a post-processing strategy based on region parameters of connected components in the binary images was adapted. The threshold values of region parameters were empirically investigated and applied separately on thick, thin and intensity transformed binary images to remove the non-vessel components. The logical OR operation is performed on the thresholded images for obtaining the segmented binary image. The DRIVE and CHASE_DB1 datasets are used for assessing the sensitivity, specificity, accuracy, AUC and MCC of the developed unsupervised approach. Comparatively, our method exhibits all-round performance on both databases and accomplishes same or even better in comparison with existing literature.

In this work, we target the class imbalance and contrast variability challenges by incorporating the multi-scale Hessian approach and modified PSO-CLAHE based contrast enhancement. The proposed method may find it challenging to segment very thin vessels especially single pixels wide. However, it results in the segmentation of some of the thin vessels which are hard to be segmented using many state-of-the-art unsupervised methods. The slight improvement in sensitivity, accuracy, and MCC is due to the segmentation of some of these thin vessels. The achieved results confirm that the developed framework can be applied for retinal blood vessel segmentation.

REFERENCES

[1] R. Klein, B. E. Klein, and S. E. Moss, "Visual impairment in diabetes," *Ophthalmology*, vol. 91, no. 1, pp. 1–9, 1984. [Online]. Available: http://www.sciencedirect.com/science/article/pii/S0161642084343378

[2] R. N. Frank, "Diabetic retinopathy," *Prog. Retinal Eye Res.*, vol. 14, no. 2, pp. 361–392, 1995. [Online]. Available: http://www.sciencedirect.com/science/article/pii/1350946294000114

[3] A. Khawaja, T. M. Khan, K. Naveed, S. S. Naqvi, N. U. Rehman, and S. J. Nawaz, "An improved retinal vessel segmentation framework using Frangi filter coupled with the probabilistic patch based denoiser," *IEEE Access*, vol. 7, pp. 164344–164361, 2019.

[4] Z. Gao, J. Li, J. Guo, Y. Chen, Z. Yi, and J. Zhong, "Diagnosis of diabetic retinopathy using deep neural networks," *IEEE Access*, vol. 7, pp. 3360–3370, 2019.

[5] S. R. Singh, S. Handa, M. Dogra, and M. R. Dogra, "Fundoscopy and malignant hypertension," *QJM, Int. J. Med.*, vol. 112, no. 4, p. 305, Nov. 2018, doi: 10.1093/qjmed/hcy248.

[6] A. Narayanan and K. Ramani, "Role of optometry school in single day large scale school vision testing," *Oman J. Ophthalmol.*, vol. 8, pp. 28–32, Feb. 2015.

[7] Y. Jiang, N. Tan, and T. Peng, "Optic disc and cup segmentation based on deep convolutional generative adversarial networks," *IEEE Access*, vol. 7, pp. 64483–64493, 2019.

[8] S. Yu, D. Xiao, S. Frost, and Y. Kanagasingam, "Robust optic disc and cup segmentation with deep learning for glaucoma detection," *Computerized Med. Imag. Graph.*, vol. 74, pp. 61–71, Jun. 2019. [Online]. Available: http://www.sciencedirect.com/science/article/pii/S0895611118305573

[9] M. Li, Q. Yin, and M. Lu, "Retinal blood vessel segmentation based on multi-scale deep learning," in *Proc. Federated Conf. Comput. Sci. Inf. Syst. (FedCSIS)*, Sep. 2018, pp. 117–123.

[10] Y. Jiang, H. Zhang, N. Tan, and L. Chen, "Automatic retinal blood vessel segmentation based on fully convolutional neural networks," *Symmetry*, vol. 11, no. 9, p. 1112, Sep. 2019.

[11] C. Kirbas and F. Quek, "A review of vessel extraction techniques and algorithms," *ACM Comput. Surv.*, vol. 36, no. 2, pp. 81–121, Jun. 2004.

[12] M. Hashemzadeh and B. A. Azar, "Retinal blood vessel extraction employing effective image features and combination of supervised and unsupervised machine learning methods," *Artif. Intell. Med.*, vol. 95, pp. 1–15, Apr. 2019. [Online]. Available: http://www.sciencedirect.com/science/article/pii/S0933365718304457

[13] K. B. Khan, A. A. Khaliq, A. Jalil, M. A. Iftikhar, N. Ullah, M. W. Aziz, K. Ullah, and M. Shahid, "A review of retinal blood vessels extraction techniques: Challenges, taxonomy, and future trends," *Pattern Anal. Appl.*, vol. 22, no. 3, pp. 767–802, Aug. 2019. Online]. Available: https://link.springer.com/article/10.1007/s10044-018-0754-8

[14] J. Almotiri, K. Elleithy, and A. Elleithy, "Retinal vessels segmentation techniques and algorithms: A survey," *Appl. Sci.*, vol. 8, no. 2, p. 155, Jan. 2018.

[15] A. D. Hoover, V. Kouznetsova, and M. Goldbaum, "Locating blood vessels in retinal images by piecewise threshold probing of a matched filter response," *IEEE Trans. Med. Imag.*, vol. 19, no. 3, pp. 203–210, Mar. 2000.

[16] B. Zhang, L. Zhang, L. Zhang, and F. Karray, "Retinal vessel extraction by matched filter with first-order derivative of Gaussian," *Comput. Biol. Med.*, vol. 40, no. 4, pp. 438–445, Apr. 2010. [Online]. Available: http://www.sciencedirect.com/science/article/pii/S0010482510000302

[17] J. Zhang, B. Dashtbozorg, E. Bekkers, J. P. W. Pluim, R. Duits, and B. M. ter Haar Romeny, "Robust retinal vessel segmentation via locally adaptive derivative frames in orientation scores," *IEEE Trans. Med. Imag.*, vol. 35, no. 12, pp. 2631–2644, Dec. 2016.

[18] D. Kumar, A. Pramanik, S. S. Kar, and S. P. Maity, "Retinal blood vessel segmentation using matched filter and Laplacian of Gaussian," in *Proc. Int. Conf. Signal Process. Commun. (SPCOM)*, Jun. 2016, pp. 1–5.

[19] N. Memari, A. R. Ramli, M. I. Saripan, S. Mashohor, and M. Moghbel, "Retinal blood vessel segmentation by using matched filtering and fuzzy C-means clustering with integrated level set method for diabetic retinopathy assessment," *J. Med. Biol. Eng.*, vol. 39, no. 5, pp. 713–731, 2018.

[20] G. Azzopardi, N. Strisciuglio, M. Vento, and N. Petkov, "Trainable COSFIRE filters for vessel delineation with application to retinal images," *Med. Image Anal.*, vol. 19, no. 1, pp. 46–57, Jan. 2015.

[21] J. Zhang, H. Li, Q. Nie, and L. Cheng, "A retinal vessel boundary tracking method based on Bayesian theory and multi-scale line detection," *Computerized Med. Imag. Graph.*, vol. 38, no. 6, pp. 517–525, Sep. 2014. [Online]. Available: http://www.sciencedirect.com/science/article/pii/S0895611114000901

[22] M. S. Miri and A. Mahloojifar, "Retinal image analysis using curvelet transform and multistructure elements morphology by reconstruction," *IEEE Trans. Biomed. Eng.*, vol. 58, no. 5, pp. 1183–1192, May 2011.

[23] J. Rodrigues and N. Bezerra, "Retinal vessel segmentation using parallel grayscale skeletonization algorithm and mathematical morphology," in *Proc. 29th SIBGRAPI Conf. Graph., Patterns Images (SIBGRAPI)*, Oct. 2016, pp. 17–24.

[24] A. Khawaja, T. M. Khan, M. A. U. Khan, and S. J. Nawaz, "A multi-scale directional line detector for retinal vessel segmentation," *Sensors*, vol. 19, no. 22, p. 4949, Nov. 2019.

[25] S. A. A. Shah, A. Shahzad, M. A. Khan, C.-K. Lu, and T. B. Tang, "Unsupervised method for retinal vessel segmentation based on Gabor wavelet and multiscale line detector," *IEEE Access*, vol. 7, pp. 167221–167228, 2019.

[26] X. Jiang and D. Mojon, "Adaptive local thresholding by verification-based multithreshold probing with application to vessel detection in retinal images," *IEEE Trans. Pattern Anal. Mach. Intell.*, vol. 25, no. 1, pp. 131–137, Jan. 2003.

[27] L. Espona, M. J. Carreira, M. Ortega, and M. G. Penedo, "A snake for retinal vessel segmentation," in *Pattern Recognition and Image Analysis*, J. Martí, J. M. Benedí, A. M. Mendonça, and J. Serrat, Eds. Berlin, Germany: Springer, 2007, pp. 178–185.

[28] B. S. Y. Lam, Y. Gao, and A. W.-C. Liew, "General retinal vessel segmentation using regularization-based multiconcavity modeling," *IEEE Trans. Med. Imag.*, vol. 29, no. 7, pp. 1369–1381, Jul. 2010.

[29] Y. Zhao, L. Rada, K. Chen, S. P. Harding, and Y. Zheng, "Automated vessel segmentation using infinite perimeter active contour model with hybrid region information with application to retinal images," *IEEE Trans. Med. Imag.*, vol. 34, no. 9, pp. 1797–1807, Sep. 2015.

[30] S. Roychowdhury, D. D. Koozekanani, and K. K. Parhi, "Blood vessel segmentation of fundus images by major vessel extraction and subimage classification," *IEEE J. Biomed. Health Informat.*, vol. 19, no. 3, pp. 1118–1128, May 2015.

[31] N. Memari, A. R. Ramli, M. I. Bin Saripan, S. Mashohor, and M. Moghbel, "Supervised retinal vessel segmentation from color fundus images based on matched filtering and AdaBoost classifier," *PLoS ONE*, vol. 12, no. 12, pp. 1–35, Dec. 2017, doi: 10.1371/journal.pone.0188939.

[32] K. A. Thakoor, X. Li, E. Tsamis, P. Sajda, and D. C. Hood, "Enhancing the accuracy of glaucoma detection from OCT probability maps using convolutional neural networks," in *Proc. 41st Annu. Int. Conf. IEEE Eng. Med. Biol. Soc. (EMBC)*, Jul. 2019, pp. 2036–2040.

[33] X. Zeng, H. Chen, Y. Luo, and W. Ye, "Automated diabetic retinopathy detection based on binocular siamese-like convolutional neural network," *IEEE Access*, vol. 7, pp. 30744–30753, 2019.

[34] Y. Muraoka, A. Tsujikawa, T. Murakami, K. Ogino, K. Kumagai, K. Miyamoto, A. Uji, and N. Yoshimura, "Morphologic and functional changes in retinal vessels associated with branch retinal vein occlusion," *Ophthalmology*, vol. 120, no. 1, pp. 91–99, Jan. 2013. [Online]. Available: http://www.sciencedirect.com/science/article/pii/S0161642012006148

[35] M. V. Cicinelli, A. Rabiolo, R. Sacconi, A. Carnevali, L. Querques, F. Bandello, and G. Querques, "Optical coherence tomography angiography in dry age-related macular degeneration," *Surv. Ophthalmology*, vol. 63, no. 2, pp. 236–244, Mar. 2018. [Online]. Available: http://www.sciencedirect.com/science/article/pii/S0039625717300590

[36] K. BahadarKhan, A. A. Khaliq, and M. Shahid, "A morphological hessian based approach for retinal blood vessels segmentation and denoising using region based otsu thresholding," *PLoS ONE*, vol. 11, no. 7, pp. 1–19, Jul. 2016, doi: 10.1371/journal.pone.0158996.

[37] M. Alhussein and S. I. Haider, "Improved particle swarm optimization based on velocity clamping and particle penalization," in *Proc. 3rd Int. Conf. Artif. Intell., Modeling Simulation (AIMS)*, Dec. 2015, pp. 61–64.

[38] G. Qinqing, C. Dexin, Z. Guangping, and H. Ketai, "Image enhancement technique based on improved PSO algorithm," in *Proc. 6th IEEE Conf. Ind. Electron. Appl.*, Jun. 2011, pp. 234–238.

[39] F. R. D. Velasco, "Thresholding using the ISODATA clustering algorithm," *IEEE Trans. Syst. Man Cybern.*, vol. 10, pp. 771–774, Nov. 1980.

[40] M. M. Fraz, S. A. Barman, P. Remagnino, A. Hoppe, A. Basit, B. Uyyanonvara, A. R. Rudnicka, and C. G. Owen, "An approach to localize the retinal blood vessels using bit planes and center-line detection," *Comput. Methods Programs Biomed.*, vol. 108, no. 2, pp. 600–616, Nov. 2012. [Online]. Available: http://www.sciencedirect.com/science/article/pii/S0169260711002276

[41] J. Staal, M. D. Abramoff, M. Niemeijer, M. A. Viergever, and B. van Ginneken, "Ridge-based vessel segmentation in color images of the retina," *IEEE Trans. Med. Imag.*, vol. 23, no. 4, pp. 501–509, Apr. 2004.

[42] J. V. B. Soares, J. J. G. Leandro, R. M. Cesar, H. F. Jelinek, and M. J. Cree, "Retinal vessel segmentation using the 2-D Gabor wavelet and supervised classification," *IEEE Trans. Med. Imag.*, vol. 25, no. 9, pp. 1214–1222, Sep. 2006.

[43] Z. Yan, X. Yang, and K.-T. Cheng, "A three-stage deep learning model for accurate retinal vessel segmentation," *IEEE J. Biomed. Health Informat.*, vol. 23, no. 4, pp. 1427–1436, Jul. 2019.

[44] R. Sundaram, K. S. Ravichandran, P. Jayaraman, and B. Venkatraman, "Extraction of blood vessels in fundus images of retina through hybrid segmentation approach," *Mathematics*, vol. 7, no. 2, p. 169, Feb. 2019, doi: 10.3390/math7020169.

[45] K. B. Khan, A. A. Khaliq, M. Shahid, and S. Khan, "An efficient technique for retinal vessel segmentation and denoising using modified isodata and clahe," *IIUM Eng. J.*, vol. 17, no. 2, pp. 31–46, Nov. 2016. [Online]. Available: https://journals.iium.edu.my/ejournal/index.php/iiumej/article/view/611

[46] J. Dash and N. Bhoi, "An unsupervised approach for extraction of blood vessels from fundus images," *J. Digit. Imag.*, vol. 31, no. 6, pp. 857–868, Dec. 2018.

[47] S. A. A. Shah, T. B. Tang, I. Faye, and A. Laude, "Blood vessel segmentation in color fundus images based on regional and hessian features," *Graefe's Arch. Clin. Experim. Ophthalmol.*, vol. 255, no. 8, pp. 1525–1533, Aug. 2017.

[48] K. B. Khan, A. A. Khaliq, and M. Shahid, "A novel fast GLM approach for retinal vascular segmentation and denoising," *J. Inf. Sci. Eng.*, vol. 33, no. 6, pp. 1611–1627, 2017.

[49] D. Marín, A. Aquino, M. E. Gegundez-Arias, and J. M. Bravo, "A new supervised method for blood vessel segmentation in retinal images by using gray-level and moment invariants-based features," *IEEE Trans. Med. Imag.*, vol. 30, no. 1, pp. 146–158, Jan. 2011.

[50] M. M. Fraz, P. Remagnino, A. Hoppe, B. Uyyanonvara, A. R. Rudnicka, C. G. Owen, and S. A. Barman, "An ensemble classification-based approach applied to retinal blood vessel segmentation," *IEEE Trans. Biomed. Eng.*, vol. 59, no. 9, pp. 2538–2548, Sep. 2012.

[51] E. Cheng, L. Du, Y. Wu, Y. J. Zhu, V. Megalooikonomou, and H. Ling, "Discriminative vessel segmentation in retinal images by fusing context-aware hybrid features," *Mach. Vis. Appl.*, vol. 25, no. 7, pp. 1779–1792, Oct. 2014.

[52] Q. Li, B. Feng, L. Xie, P. Liang, H. Zhang, and T. Wang, "A cross-modality learning approach for vessel segmentation in retinal images," *IEEE Trans. Med. Imag.*, vol. 35, no. 1, pp. 109–118, Jan. 2016.

[53] J. I. Orlando, E. Prokofyeva, and M. B. Blaschko, "A discriminatively trained fully connected conditional random field model for blood vessel segmentation in fundus images," *IEEE Trans. Biomed. Eng.*, vol. 64, no. 1, pp. 16–27, Jan. 2017.

[54] A. Dasgupta and S. Singh, "A fully convolutional neural network based structured prediction approach towards the retinal vessel segmentation," in *Proc. IEEE 14th Int. Symp. Biomed. Imag. (ISBI)*, Apr. 2017, pp. 248–251.

[55] Z. Yan, X. Yang, and K.-T. Cheng, "Joint segment-level and pixel-wise losses for deep learning based retinal vessel segmentation," *IEEE Trans. Biomed. Eng.*, vol. 65, no. 9, pp. 1912–1923, Sep. 2018.

[56] S. Y. Shin, S. Lee, I. D. Yun, and K. M. Lee, "Deep vessel segmentation by learning graphical connectivity," *Med. Image Anal.*, vol. 58, Dec. 2019, Art. no. 101556. . [Online]. Available: http://www.sciencedirect.com/science/article/pii/S1361841519300982

[57] Y. Jiang, N. Tan, T. Peng, and H. Zhang, "Retinal vessels segmentation based on dilated multi-scale convolutional neural network," *IEEE Access*, vol. 7, pp. 76342–76352, 2019.

[58] D. Adapa, A. N. J. Raj, S. N. Alisetti, Z. Zhuang, and G. Naik, "A supervised blood vessel segmentation technique for digital fundus images using zernike moment based features," *PLoS ONE*, vol. 15, no. 3, pp. 1–23, Mar. 2020, doi: 10.1371/journal.pone.0229831.

[59] X. You, Q. Peng, Y. Yuan, Y.-M. Cheung, and J. Lei, "Segmentation of retinal blood vessels using the radial projection and semi-supervised approach," *Pattern Recognit.*, vol. 44, nos. 10–11, pp. 2314–2324, Oct. 2011. [Online]. Available: http://www.sciencedirect.com/science/article/pii/S0031320311000161
[60] P. Bankhead, C. N. Scholfield, J. G. McGeown, and T. M. Curtis, "Fast retinal vessel detection and measurement using wavelets and edge location refinement," *PLoS ONE*, vol. 7, no. 3, pp. 1–12, Mar. 2012, doi: 10.1371/journal.pone.0032435.
[61] B. Yin, H. Li, B. Sheng, X. Hou, Y. Chen, W. Wu, P. Li, R. Shen, Y. Bao, and W. Jia, "Vessel extraction from non-fluorescein fundus images using orientation-aware detector," *Med. Image Anal.*, vol. 26, no. 1, pp. 232–242, Dec. 2015. [Online]. Available: http://www.sciencedirect.com/science/article/pii/S1361841515001395
[62] A. Ali, W. M. D. W. Zaki, and A. Hussain, "Blood vessel segmentation from color retinal images using K-means clustering and 2D Gabor wavelet," in *Proc. Int. Conf. Appl. Phys., Syst. Sci. Comput.*, 2018, pp. 221–227.
[63] S. Roychowdhury, D. Koozekanani, and K. Parhi, "Blood vessel segmentation of fundus images by major vessel extraction and subimage classification," *IEEE J. Biomed. Health Informat.*, vol. 19, no. 3, pp. 1118–1128, May 2015.
[64] A. M. Mendonca and A. Campilho, "Segmentation of retinal blood vessels by combining the detection of centerlines and morphological reconstruction," *IEEE Trans. Med. Imag.*, vol. 25, no. 9, pp. 1200–1213, Sep. 2006.
[65] Y. Zhao, Y. Liu, X. Wu, S. P. Harding, and Y. Zheng, "Retinal vessel segmentation: An efficient graph cut approach with retinex and local phase," *PLoS ONE*, vol. 10, no. 4, pp. 1–22, Apr. 2015, doi: 10.1371/journal.pone.0122332.
[66] L. C. Rodrigues and M. Marengoni, "Segmentation of optic disc and blood vessels in retinal images using wavelets, mathematical morphology and hessian-based multi-scale filtering," *Biomed. Signal Process. Control*, vol. 36, pp. 39–49, Jul. 2017. [Online]. Available: http://www.sciencedirect.com/science/article/pii/S1746809417300629

MUSAED ALHUSSEIN received the B.S. degree in computer engineering from King Saud University (KSU), Riyadh, Saudi Arabia, in 1988, and the M.S. and Ph.D. degrees in computer science and engineering from the University of South Florida, Tampa, FL, USA, in 1992 and 1997, respectively. Since 1997, he has been on the Faculty of the Computer Engineering Department, College of Computer and Information Science, KSU. Recently, he has been successful in winning a research project in the area of AI for healthcare, which is funded by the Ministry of Education at Saudi Arabia. He is the Founder and Director of the Embedded Computing and Signal Processing Research (ECASP) Laboratory. He is currently a Professor with the Department of Computer Engineering, College of Computer and Information Sciences, KSU. His research activity is focused on typical topics of computer architecture and signal processing, with an emphasis on big data, machine/deep learning, VLSI testing and verification, embedded and pervasive computing, cyber-physical systems, mobile cloud computing, big data, eHealthcare, and body area networks.

KHURSHEED AURANGZEB (Senior Member, IEEE) received the B.S. degree in computer engineering from the COMSATS Institute of Information Technology Abbottabad, Pakistan, in 2006, the M.S. degree in electrical engineering (system on chip design) from Linkoping University, Sweden, in 2009, and the Ph.D. degree in electronics design from Mid Sweden University Sweden, in June 2013. He has authored and coauthored more than 68 publications, including IEEE/ACM/Springer/Hindawi/MDPI journals, and flagship conference papers. He has obtained more than ten years of excellent experience as instructor and researcher in data analytics, machine/deep learning, signal processing, electronic circuits/systems, and embedded systems. He is currently an Assistant Professor with the College of Computer and Information Sciences, King Saud University (KSU), Riyadh, Saudi Arabia. He has been involved in many research projects as a principal investigator and a co-principal investigator. His research interest are in the diverse fields of embedded systems, computer architecture, VLSI, signal processing, wireless sensor networks, camera-based sensor networks, and smart grids with an emphasis on big data, precision agriculture, machine/deep learning, embedded and pervasive computing, mobile cloud computing, and healthcare.

SYED IRTAZA HAIDER received the B.E. degree in electronics engineering from the National University of Sciences and Technology (NUST), Pakistan, in 2010, and the M.S. degree in electronics engineering from King Saud University (KSU), Saudi Arabia, in 2015. He is currently a Researcher with the Embedded Computing and Signal Processing Lab (ECASP), KSU. His research interests include artificial intelligence, machine learning, deep learning, healthcare, smart grids, signal processing, and mixed signal design.